Eur. Phys. J. Appl. Phys. **41**, 205–213 (2008)
DOI: 10.1051/epjap:2008019

THE EUROPEAN PHYSICAL JOURNAL APPLIED PHYSICS

A new p^+-i-n^+ photodiode SPICE model for CMOS pixel applications

R. Negru[a], Y. Bonnassieux, S. Tchakarov, and P.R. i Cabarrocas

LPICM Ecole Polytechnique, 91128 Palaiseau Cedex, France

Received: 7 December 2007 / Received in final form: 18 December 2007 / Accepted: 21 December 2007
Published online: 12 March 2008 –

Abstract. In this paper we discuss and model the effects of the density of defects in hydrogenated amorphous silicon from an electronics point of view. To this end, we have created a SPICE model that accounts for the two main field effects, Poole-Frenkel and tunnel, responsible for the leakage current. The comparison between our model and the experimental data shows that our approach allows a quick evaluation of the quality of the device with no need to run a complete steady state measurement. Also, we have validated our SPICE photodiode model by implementing it into a three CMOS simple pixel structure.

PACS. 85.60.Dw Photodiodes; phototransistors; photoresistors – 85.60.-q Optoelectronic devices

Introduction

High-quality amorphous/polymorphous silicon p^+-i-n^+ photodiodes show very small dark leakage current, allowing the detection of low intensity illuminations with a dynamic range of several orders of magnitude [1,2]. Those qualities, compatible with the CMOS[1] technology, position them as good candidates for the achievement of very high efficiency optical sensors [3,4]. Due to the complexity and the countless mechanisms which describe the behaviour of a pixel based on a p^+-i-n^+ diode, our interest in the use of the p^+-i-n^+ photodiode in sensor matrix applications involves the analysis and the optimisation of such devices by a complete simulation process. In this paper we propose a 1D SPICE [5,6] model for a p^+-i-n^+ photodiode based on two main assumptions. First, the planar symmetry of the surface of the pixel allows to transform a 3D problem (width, length and depth) into a 2D problem (length and depth). Second, the high ratio length/depth allows to neglect the border effects, thus to go from a 2D model to a 1D model where only the depth effects are taken into consideration. In the following we refer the depth as the z axis.

The content of this paper is divided into four parts. In the first part we present the main physical effects that account for the leakage current as well as the formalism used to model them.

In the second part we present a procedure based on the analysis of dark and light current/voltage characteristics to extract the physical parameters.

The light excitation model is presented in the third part. A separated block simulate the photodiode response to a uniform white light pulsed excitation. We specify the absence of the spectral behaviour from this model.

Finally, the fourth part shows how the model can be applied to simulate the integration of the photodiode in a three CMOS pixel structure.

1 Formalism and field effects

p^+-i-n^+ photodiodes realized in a-Si:H have, in reverse polarization (around -1 V), a very weak dark current ($\sim$10 pA/cm^2) [1]. This property is extremely useful as it allows high light sensitivity together with a very large dynamic range. In order to model the response of the photodiode it is necessary to understand the physical phenomena that give rise to the dark current. To do so, we review here the formalism from the base of our calculations together with the two field mechanisms that influence the hole-electron pair thermal generation: the *Poole-Frenkel* [7] and *tunnel* [8] effects.

1.1 Steady state leakage current formalism

Lemmi [9] has given an extended expression to model the effect of the electric field on the steady state current of a p^+-i-n^+ photodiode under reverse bias:

$$I(V) = qN_D AdkTw_0 e^{(-E_C - E_{FD}(V))/kT} f(V) \quad (1)$$

Where q is the electron charge, N_D the average density of defects, A the sensor surface, d the i-layer thickness, k the

[a] e-mail: razvan.negru@polytechnique.edu
[1] Complementary Metal Oxide Semiconductor

Boltzmann constant, T the absolute temperature, w_0 the emission rate pre-factor, E_C the conduction band energy and the E_{FD} is the quasi-Fermi energy, describing the occupancy of the band-gap. $f(V)$ is the field enhancement term[2]:

$$f(V) \cong e^{\Delta E(V)/kT} \frac{V + V_{BTIN}}{V} \quad (2)$$

where V_{BTIN} is the built-in-potential of the junction and $\Delta E(V)$ is the decrease of the barrier to the emission of trapped electron for a V voltage. The rightmost factor in e.g. (2) accounts for non-uniform emission in the i-layer at low bias.

The emission of a trapped electron from a Coulomb well in presence of an electric field (Poole-Frenkel effect) is accompanied by the emission of a hole to the valence band, through the tunnel effect [10]. The emission probability is a function of the energy depth in the gap. For a given voltage, E_{FD} can be found by equating the emission probabilities to the conduction and valence band. Equations[3]:

$$\Delta E_{PF}(V) = q\sqrt{\frac{q\,(V + V_{BTIN})}{\pi\varepsilon d}} \quad (3)$$

$$\Delta E_{TUN}(V) = qR_T \frac{V + V_{BTIN}}{d} \quad (4)$$

give the decrease of the emission energy barrier as a function of a voltage, V, due to the Poole-Frenkel and tunnel effects respectively; ε is the permittivity of a-Si:H, V_{BTIN} is the junction potential, d is the i-layer thickness and R_T is the tunnel length.

After this short review of the Lemmi's formalism [9], used as the basis of our model, let us first propose a simplification of the former model, such as taking the value of E_{FD} constant. In fact E_{FD} is the energetic level at which the probability of occupation of a state by a charge is 50%. We can talk about two quasi-Fermi levels, one for holes E_{FDp} and one for electrons E_{FDn}, in the case of an extrinsic semiconductor where the volume number of free electrons is different from one of free holes (here we talk about currents of drift and diffusion). This happens when an electrical field is applied or where the structure is doped. If we neglect the drift and diffusion current we can suppose that our semiconductor is at equilibrium and it is intrinsic, in this case the Fermi level is equal with the intrinsic Fermi level which is the mid-gap. This simplification facilitates also the convergence of the SPICE numerical routines to a stable solution.

In consequence, the saturation current, I_S, will be represented by the following expression:

$$I_S = qN_D AdkTw_0 e^{-\frac{E_G}{2kT}} \quad (5)$$

given by e.g. (1) where the $E_{FD} = -(E_C + E_V)/2$, i.e. the mid-gap, and the gap is $E_G = E_C - E_V$, where E_V is the valence band energy. So the exponential term becomes constant.

Using usual values for a-Si:H material and our photodiode structure: $N_D = 5\times10^{15}$ cm^{-3}eV^{-1}, $A = 0.25$ mm^2, $d = 0.5$ μm, $T = 300$ K, $w_0 = 10^{13}$ s^{-1}, $E_G = 1.8$ eV, we obtain 21 fA for I_S. This calculated I_S value is close to our measured value, 50 fA (see Sect. 2.2.1).

Another approach that we have introduced in e.g. (2) is related to the non-uniform emission in the i-layer at low bias, that allows to substitute Lemmi $f(V)$ by the transfer function of a given circuit. A detailed discussion of this circuit will be presented in Section 2.3.

In the following section we present the physical phenomena caused by the two-field effects at the basis of the steady state leakage current.

1.2 Poole-Frenkel effect

In general there are two main effects that can explain the release of an electron trapped in a Coulomb well due to the electric field, the Poole-Frenkel and the tunnel effects. The Poole-Frenkel effect can be represented by a diminution of the Coulomb potential barrier when an external electrical field is applied. In fact, the Poole-Frenkel effect represents the decrease of a potential barrier of a charged capture level in a semiconductor or in an isolator. As a consequence, the Poole-Frenkel effect increases the emission frequency of carriers (electrons or holes) starting from *initially neutral states* [10].

For simplicity, we have uncoupled graphically the Poole-Frenkel and the tunnel effects to explain the leakage current. Figure 2 shows the Poole-Frenkel effect for a Coulomb well situated in the conduction band (CB).

According to the figure, in absence of the tunnel effect, a Poole-Frenkel effect strong enough ($\Delta E_{PF\ strong}$) can release the electron out of the potential well, whereas a weaker effect ($\Delta E_{PF\ weak}$) will only send the electron to a bound state into the well. E is the energy axis and z is the modelling axis (depth of the photodiode structure previously defined in Fig. 1). E_t is the transition level, which is a function of the nature of a particular defect. $E_{vl} = E_C(0) - Fz$ is the virtual level energy at the point z, where $E_C(0)$ is the conduction band energy level at z=0 point and F (V/cm) is the applied electrical field.

1.3 Tunnel effect

Transitions due to the tunnel effect can occur either from *neutral* or from *charged states,* whereas the Poole-Frenkel can take place only from neutral states. Depending on the origin of the tunnel effect we can talk about either pure or phonon-assisted tunnel effect [8,10].

The pure tunnel effect corresponds to the tunnelling of electrons (or holes) caught in the deep levels towards the conduction (or valence) band situated at the same energy called "horizontal" transitions (see Fig. 3).

Regarding the phonon-assisted tunnel effect, we refer to the Vincent approach [8], which is based on the

[2] This equation is the correction of the one from Lemmi's article.

[3] This equation is not the one from Lemmi's article. It is the Poole-Frenkel equation in eV.

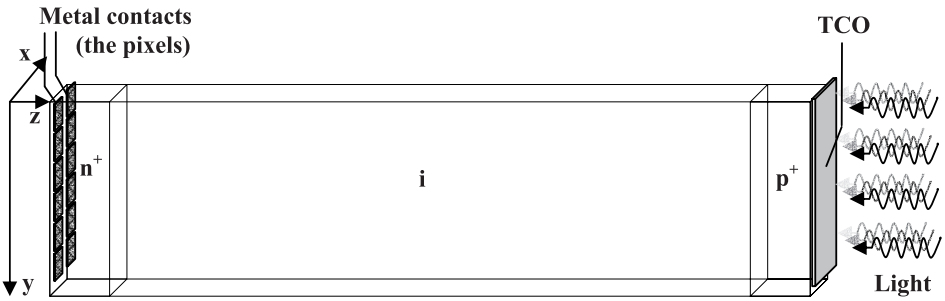

Fig. 1. Layout of a p^+-i-n^+ optical sensor. We can see that the light comes from right, entering the transparent conducting oxide (TCO). It is absorbed in the p^+, i and n^+ layers. The photogenerated current is collected at the metal and ITO contacts of the pixels.

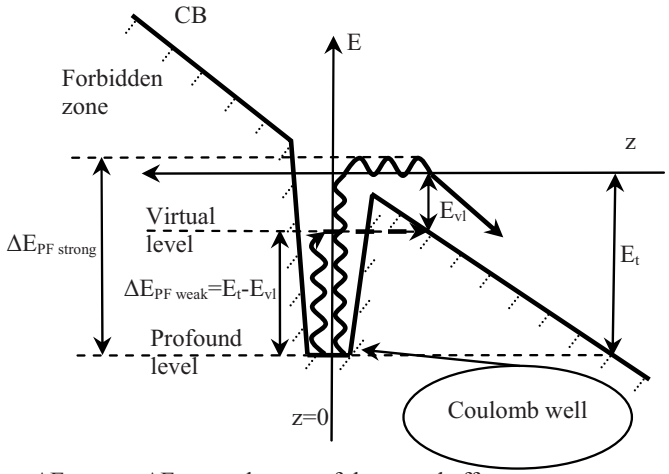

Fig. 2. Poole-Frenkel effect in a Coulomb well.

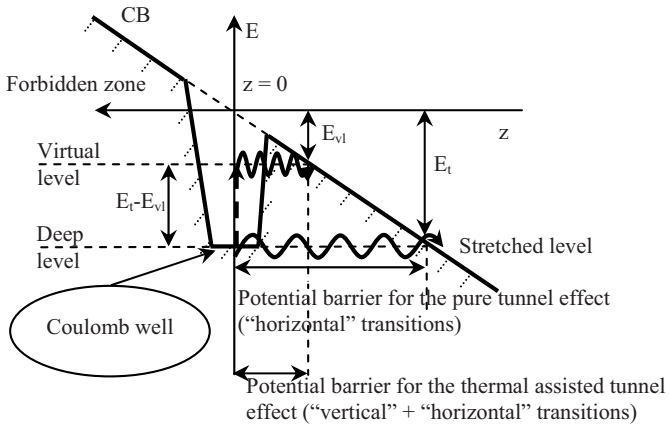

Fig. 3. Tunnel effect in a Coulomb well.

virtual level concept in the band gap ("vertical" transition, = thermal effect, + "horizontal" transition, = tunnel effect). The probability of a thermal-assisted tunnel transition from a deep level E_t is the product of the probability of a thermal transition from E_t to the virtual level E_{vl}, by the probability of a pure tunnel transition from E_{vl} to the conduction (valence) band. The difference between them is in fact that the treated transitions are the horizontal ones (i.e. at the same energy level).

In practice the Poole-Frenkel and the tunnel effects are coupled, here, we have presented them separately for clarity, but if we want to model the leakage currents we have to consider them as a whole ($\Delta E_{PF} + \Delta E_{TUN}$).

2 Model implementation (static components and dynamical model)

The dark current in reverse polarization gives the dynamical range of a p^+-i-n^+ junction. Theoretically, the inferior limit of this range is set by the leakage current due to the thermal generation processes. The $I(V)$ characteristic is the most common criterion to evaluate the performances of any kind of photodiode.

The $I(V)$ characteristic curve is obtained by measuring the current which passes through the photodiode using a polarization voltage slope. The measurement must be performed in the dark and under illumination. The voltage range is chosen in order to obtain both the direct and reverse polarization working modes.

In our particular case, to obtain the $I(V)$ characteristics, the polarization voltage interval was set from -3 V to 1 V, with a 0.01 V step resolution and a 1s delay between steps to ensure stabilization. The current measurements were realized by integrating, "n" electrical periods at 50 Hz.

2.1 Model achievement

2.1.1 Physical parameters measure

Measured dark $I(V)$ characteristics lie at the basis of our modelling [1,2]. Generally, the dark $I(V)$ characteristics are divided into three zones: the direct polarization zone, the transition zone (important for the dynamical circuit) and the negative reverse polarization zone. Figure 4 illustrates the physical parameters that can be extracted from a typical $I(V)$ characteristic curve: the serial resistance (R_S), the saturation current (I_S), the ideality factor (N),

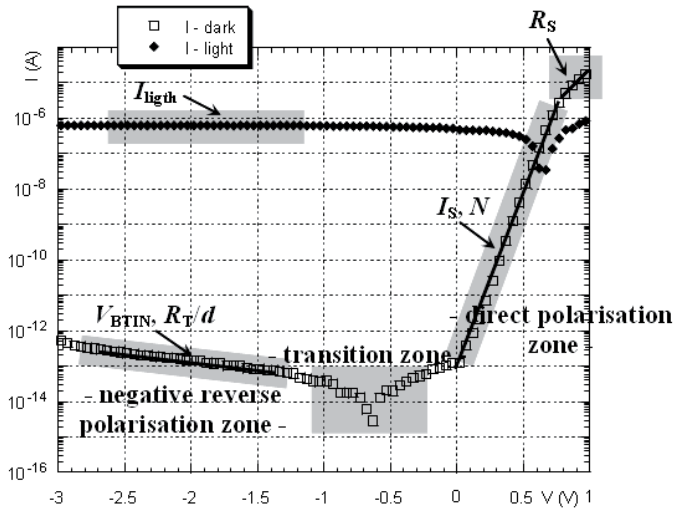

Fig. 4. Main physical parameters that can be extracted from $I(V)$ characteristics measured under dark and illumination conditions. The intensity axis is represented in logarithmical scale.

the ratio between the size of the potential barrier of the tunnel effect and the thickness of the i-layer (R_T/d), and the junction potential (V_{BTIN}).

In Figure 4, we have also represented the $I(V)$ characteristics under illumination. From this curve, we have chosen the voltage interval $[-2.6, -1.2\,\mathrm{V}]$ to extract the light current value, I_{light} ($\cong 0.8\,\mu\mathrm{A}$). Along this voltage interval, also called the working zone, we notice that under continuous, uniform and white lighting, I_{ligth} is practically constant if represented in a logarithmic scale.

In practice the photodiode is operated in reverse mode in order to enhance photocurrent efficiency and to avoid direct polarization current, which is more important than the reverse current.

2.1.2 Equivalent circuit of our photodiode

SPICE allows the customization of electronic components using predefined component libraries [5,6]. The circuit of Figure 5, which describes our photodiode, is conceived using a combination of different basic electronic components.

In the circuit of Figure 5, the *dark current* was simulated by two voltage current generators, one for the direct polarization (I_{dd} – direct dark) and the other for the reverse polarization (I_{rd} – reverse dark). The *light current*, I_{ligth}, was simulated with only one generator (I_l). We specify that the polarization tension for the dark current block is different from the one for the light current block (V_l – lightning effect voltage), but the outputs of these two blocks are connected. The *response due to a light pulse*, was simulated by means of a specific circuit placed between the light current generator I_l and the lightning effect voltage V_l (see Sect. 3). From our experimental measurements we noticed an inversion of the photodiode current sign for negative potentials (see in Fig. 4 the dark current transitory zone). The feature located in the *transition zone* of the $I(V)$ characteristic curve was simulated with a parallel circuit (made of OA[4], $R\ d/dt$ and I_{te} – transitory effect). The objective of this circuit is to model the non linear behaviour in voltage of the photodiode parallel capacity and resistance. To do so, we have put in the OA the function $f(V,C)$ that best fits the capacity nonlinear behaviour. As a result, the circuit has the role to shift the zero point position of the $I(V)$ (it replaces the rightmost factor from e.g. (1), i.e. $f(V)$, and it is based upon the idea of a parallel *series RC*). *The series resistance* (R_S) is situated before the current output, which represents our simulation circuit answer. This circuit was associated to the symbol represented in Figure 6.

2.2 Static components

We consider as static components *the dark current* and *the series resistance*.

2.2.1 Dark current under direct polarisation

Our definition of the dark current in direct polarisation is based on the classic formula:

$$I = I_S\left(e^{\frac{qV}{NkT}} - 1\right) \tag{6}$$

where I_S is the saturation current, q the electrical charge, V the polarization voltage, k the Boltzmann constant, T the absolute temperature and N the ideality factor.

In order to calculate I_S we made the following approximation:

$$I \cong I_S e^{\frac{qV}{NkT}} \tag{7}$$

then, using the empirical $I(V)$ characteristics (Fig. 4) between 0 and 0.7 V, we can determine the values of I_S and the ratio $\frac{q}{NkT}$ to be ($\cong$50 fA) and ($\cong 24\,\mathrm{V}^{-1}$) respectively. If we define the following constants:

$$M_0 = I_S \quad \text{and} \quad M_1 = \frac{q}{NkT} \tag{8}$$

we can rewrite the expression (7) as:

$$I = M_0 e^{M_1 V}. \tag{9}$$

Knowing the values of q, k and T (300 K), we can find the value of the ideality factor, N ($\cong$1.6).

In general, we simulate the dark current under direct polarization through a voltage-controlled current source with the following equation:

$$I = M_0(e^{M_1 V} - 1). \tag{10}$$

From 0.8 V to 1 V the behaviour of the $I(V)$ characteristic curve is dominated by the Joule effect. This fact allows determining the value of *the series resistance*, R_S, which we

[4] OA – operational amplifier.

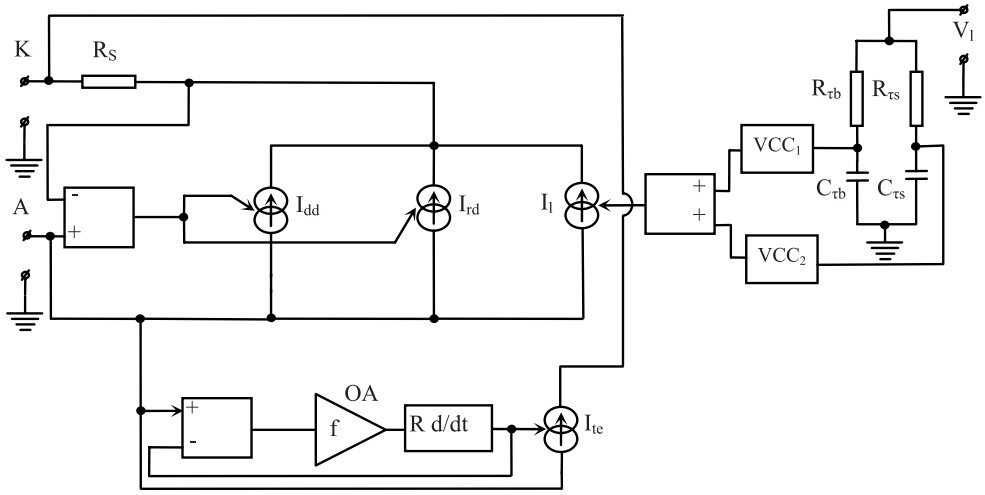

Fig. 5. SPICE layout of the equivalent circuit of our photodiode.

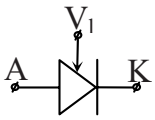

Fig. 6. Symbol associated with the simulation circuit (A-anode, K-cathode and V_l-voltage that models the effect of the illumination of the photodiode).

suppose to be constant in our model. To do so in practice, we fit a straight line given by:

$$I = M_2 + M_3 V \tag{11}$$

where M_2 has no physical meaning and R_S is related to M_3 by:

$$R_S \cong \frac{1}{M_3} \tag{12}$$

(for our photodiode the value of R_S is almost 12 kΩ).

2.2.2 Dark current under reverse polarisation

As we can see in Figure 5, at the basis of the dark current stays two voltage-controlled current generators: I_{dd} and I_{rd}.

I_{dd} also called $I_{direct\text{-}dark}$ is due to the photodiode direct polarization:

$$I_{direct\text{-}dark} = I_S(e^{\frac{qV}{NkT}} - 1) \tag{13}$$

as has been previously stated in Section 2.2.1.

I_{rd} also called $I_{reverse\text{-}dark}$, is due to the reverse polarization:

$$I_{reverse\text{-}dark} = I_S(e^{\frac{qV}{NkT}} - 1)e^{\frac{\Delta E_{PF}+\Delta E_{TUN}}{2kT}}. \tag{14}$$

The second exponential accounts for the Poole-Frenkel and tunnel effects (see e.g. (3) and e.g. (4)), the addition $\Delta E_{PF} + \Delta E_{TUN}$ represents the fact that both effects are coupled.

In reverse mode and small voltages in absolute value, we can consider that the Poole-Frenkel effect is negligible compared to the tunnel effect. Then, in order to obtain the tunnel effect parameter ΔE_{TUN}, we have taken the absolute value of e.g. (14) and then rewritten it as follows:

$$abs(I) = I_0 e^{\frac{(V+V_{BTIN})qR_T}{2dkT}} \tag{15}$$

where $I_0 = I_S(e^{\frac{qV}{NkT}} - 1)$. In reverse polarization the exponential is negligible, reason why I_0 can be considered as a constant, i.e. $I_0 = I_S$, as it has already stated (see e.g. (9)). In practice, we have chosen a voltage interval for which the measured $I(V)$ characteristic curve will be linear in a logarithmic scale. This interval, which is going to be the standard operation mode of the photodiode, is bounded between −2.6 V and −1.2 V (see Fig. 4). The experimental points of the $I(V)$ characteristic can be adjusted using the following function:

$$abs(I) = M_4 e^{M_5 V}. \tag{16}$$

Then after equating expressions (16) and (15) we can obtain the following equivalences:

$$M_4 = I_S e^{\frac{V_{BTIN}qR_T}{2dkT}} \quad \text{and} \quad M_5 = \frac{qR_T}{2dkT}. \tag{17}$$

The best-fitted values of M_4 and M_5 are: $M_4 = 1.676210^{-14}$ A and $M_5 = -1.0727\,\mathrm{V}^{-1}$. We can then deduce the following expression for V_{BTIN}:

$$V_{BTIN} = \frac{\ln\ M_4 - \ln\ I_S}{M_5} \tag{18}$$
$$(V_{BTIN} = 1.0188\,\mathrm{V}).$$

Therefore:

$$\frac{\Delta E_{TUN}}{2kT} = V M_5 + \ln\ M_4 - \ln\ I_S. \tag{19}$$

Once the value of V_{BTIN} is known; the Poole-Frenkel effect parameter, ΔE_{PF}, has been calculated using e.g. (3):

$$\frac{\Delta E_{PF}}{2kT} = \frac{q}{2kT}\sqrt{\frac{q\,(V+V_{BTIN})}{\varepsilon\pi d}} \cong 0.5996\sqrt{V+V_{BTIN}} \tag{20}$$

d is the thickness of the intrinsic layer (in our case it is 0.5 μm), and ε is the a-Si:H permittivity.

Then we can conclude that the dark current is obtained by the addition:

$$I_{dark} = I_{direct\text{-}dark} + I_{reverse\text{-}dark}. \tag{21}$$

2.3 Dynamic model components (Transition zone)

An important feature of the $I(V)$ characteristic curve is the transition zone (see Fig. 4), where the intensity passes from negative to positive. In our case the transition occurs around -0.7 V. In order to model the position of the transition zone as a function of the voltage, we have added a parallel circuit consisting of an OA, an $R\ d/dt$ and I_{te} (see Fig. 5).

The physical parameters that define the position of the transition zone are parallel resistance, the spatial charge zone capacity for a nonzero polarization, and the dynamic capacity of the photodiode. Because of the dynamic capacity, the photodiode parallel capacity has a voltage nonlinear response, which is the reason why we had to use the parallel circuit.

The value of the parallel capacitance, $C = C(v)$, depends on the applied voltage, v. If we note as u_C the potential drop across the capacitor, we obtain for an equivalent series RC circuit the following equation:

$$v = iR + u_C \tag{22}$$

where i is the current intensity that passes through the series RC circuit.

The voltage across the capacitor is a function of current integrated over time, so for u_C we obtain:

$$u_C = \frac{1}{C(v)}\int i\ dt. \tag{23}$$

From which we can obtain the following expression for the current intensity:

$$i = C(v)\frac{du_C}{dt}. \tag{24}$$

Because we want to use the voltage as variable, we have multiplied both sides of e.g. (24) by R, thus obtaining:

$$iR = C(v)R\frac{du_C}{dt}. \tag{25}$$

Regarding the parallel circuit, the decrease of potential described by e.g. (22), $u_C = v - iR$, is caused by the differential circuit before the OA (see Fig. 5).

The voltage, v, appears in the expression of the C, but also in the expression of u_C, so we decided to apply the non-linear behaviour only to the u_C, and obtained the following expression:

$$i = \frac{1}{R}\left(RC\frac{d}{dt}f\,(v - iR)\right) \tag{26}$$

with:

$$f(v) = 1 + (-10v)^{1/4}\left(2 + 4e^{-0.3(v-0.5)^2}\right) \tag{27}$$

where f is the mathematical function that best fits the real behaviour of the capacitor. So, the OA applies the function $Cf(v)$, C is a constant and it is not affected by the derivation.

The component connected in series with the OA, $R\ d/dt$, performs the operation $R\frac{d(Cf(v))}{dt}$.

Finally, the I_{te} is controlled by the $R\ d/dt$ output voltage that will be divided by R (i.e. globally we have for our current the form from e.g. (26)).

The numerical values for R and C were found empirically after successive simulations.

3 Model of the light impulse response

Regarding the $I(V)$ characteristic measured under illumination, (Fig. 4), we notice that in the working zone of our photodiode, its value is almost constant. Accordingly, we can obtain the value for I_{light}, that in our simulation multiplies the voltage-controlled current source that represents the light excitation (I_l from Fig. 5). We used as a source of illumination an ordinary light bulb.

Although the spectral response has not been realized here, it can be implemented using a filter on the input of the lighting effect voltage.

The dynamical part of the behaviour under illumination was simulated in terms of a light impulse response. To do so, we put the photodiode in the dark reverse polarization (a voltage around -1 V). After a long stabilization time we sent a short pulse of white light and measured the current return to the anterior equilibrium state as a function of time. The curve shown in Figure 7 gives the measured response for a p^+-i-n^+ photodiode from VAIC1C type (this measurement was realized in collaboration with CEA/LETI).

The circuit needed to model the response to the light impulse of the photodiode was interposed between the lighting effect voltage input and the voltage-controlled current source commanded by this one (i.e. between V_l and I_l from Fig. 5). We notice, from the measured response, two features. The first one is characterized by an abrupt decrease. The second feature depicts a second decrease, slower than the first. Both features were simulated using two RC circuits with time constants of 1 μs ($R_{\tau s}$, $C_{\tau s}$) and 0.2 s ($R_{\tau b}, C_{\tau b}$) respectively. Both RC circuits are connected to two voltage correction circuits, VCC_1 and VCC_2, whose role is to correct the intensity level (I_l) of the fast and slow responses in order to match them for a constant tension (V_l) of 1 V. This observation is interesting because we will look for a V_l around 1 V for tracing our $I(V)$ under illumination.

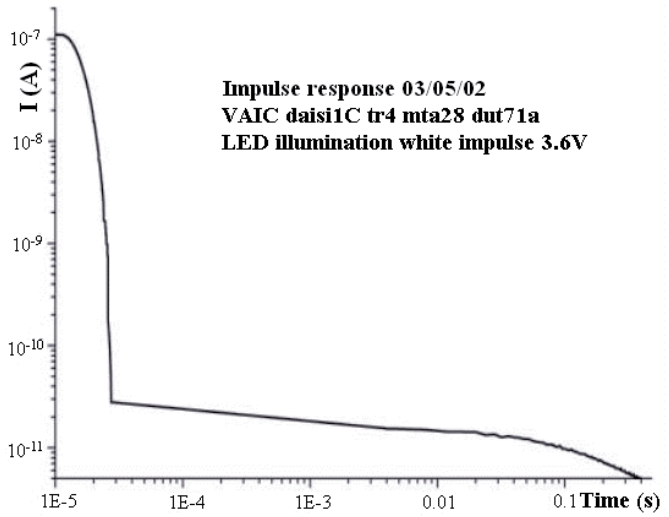

Fig. 7. Response measured after a light impulse.

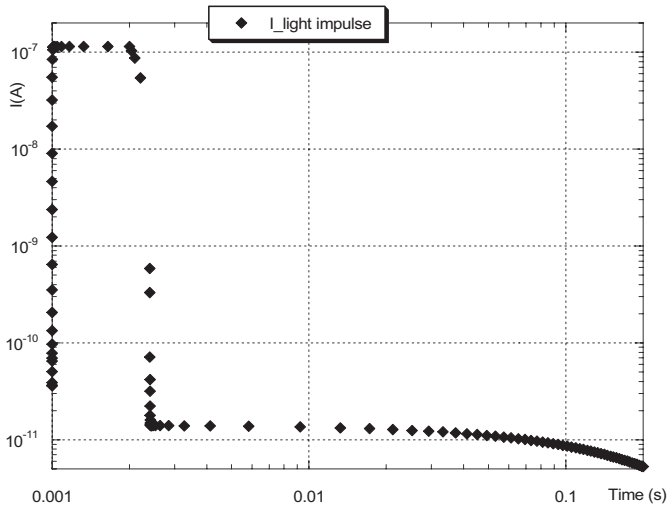

Fig. 8. Simulated response of a light impulse.

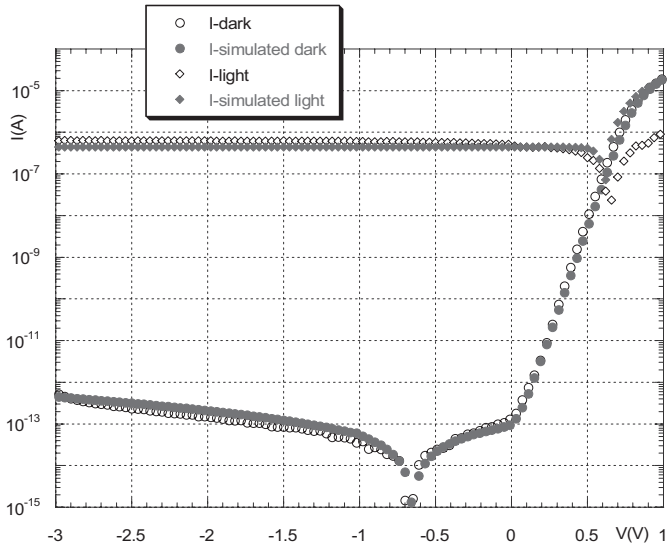

Fig. 9. Collation between the features measured and the simulated ones, both under the dark and illumination conditions.

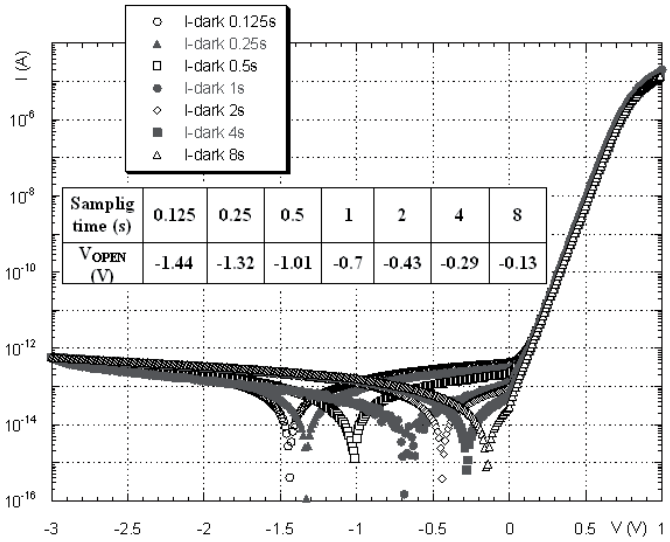

Fig. 10. Simulated static responses for different sampling times.

4 Model validation

4.1 Simulation of photodiode I(V) characteristics

In order to validate our results we traced the $I(V)$ characteristic under dark and illumination conditions. We used a voltage stimulus between −3 V and 1 V with a step of 0.01 V and a delay of 1 s, which is identical to how the real measurement was done (see chapter 2).

In Figure 9 the experimental and the simulated $I(V)$ characteristics for both the dark and the illumination conditions are shown.

The simulated characteristics fit well to the real ones. The value of V_l (Fig. 5), used to simulate the light response, was 1 V. In that way, the dynamic range of the response of the photodiode to the light is bounded between 0 and 1 V. This result is coherent with our original expectations (see the observation made before the Fig. 8).

Another interesting aspect is the static answer that consists in the comparison between several $I(V)$ characteristics measured with identical voltage steps but for different delay times. From those measurements we have observed that the shorter the sampling time is, the bigger the shift of the zero current passing voltage (V_{OPEN}) from zero is. For long sampling times, the zero passing voltage tends towards 0 V. This behaviour is related to the density of defects in the a-Si:H material which was used to make the photodiode. In general, for current photodiodes, with a high density of defects, the $I(V)$ measurements with small sampling periods are eloquent, but for high quality photodiodes alternative methods are recommended.

The different delay times, used in the simulations shown in Figure 10, were: 0.125, 0.25, 0.5, 1 (our reference), 2, 4 and 8 s.

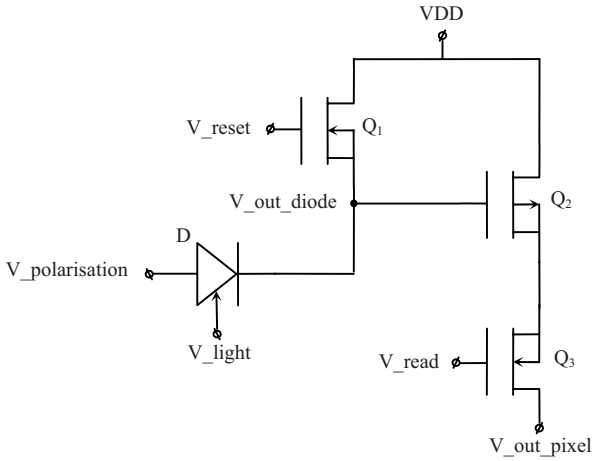

Fig. 11. Layout of a 3 CMOS pixel using our photodiode model.

In conclusion, we can say that the model represents accurately the behaviour of a real photodiode under both dark and illumination conditions.

4.2 Photodiode model integration within a pixel structure

For illustration purposes we show an example of the use of our photodiode model. In this example the photodiode is integrated within a pixel made with 3 CMOS transistors [4] represented in Figure 11.

Regarding Figure 11, D is our photodiode, Q_1, Q_2 and $Q_3$are the pixel CMOS transistors. V_polarisation is the polarisation voltage for our photodiode, whose value is in the range $[-2.6, -1.2]$ V, V_light is the voltage that simulates the light excitation, which corresponds to V_l from Figure 5, and whose value is in the range $[0, 1]$ V. VDD is the CMOS transistors polarisation voltage, in our case it is -0.6 V. V_reset is the reset voltage signal for Q_1; here, the reset is set at the VDD value. V_read is the reading voltage signal for our pixel and controls the Q_3 CMOS transistor. V_out_photodiode is the voltage that comes out from the photodiode and that controls the Q_2 gate. V_out_pixel is the output voltage signal of the pixel circuit.

Figure 12 shows the input and the output signals of the pixel.

From Figure 12 we can conclude that the output voltage signal of the photodiode is inverted with respect to the sign of the lighting effect voltage. In addition, the CMOS pixel follows proportionally the photodiode signal. So we can conclude that we have successfully integrated our photodiode model into a main pixel structure.

Conclusions

In this article we presented a new model for a photodiode. The model is based mainly on two physical effects,

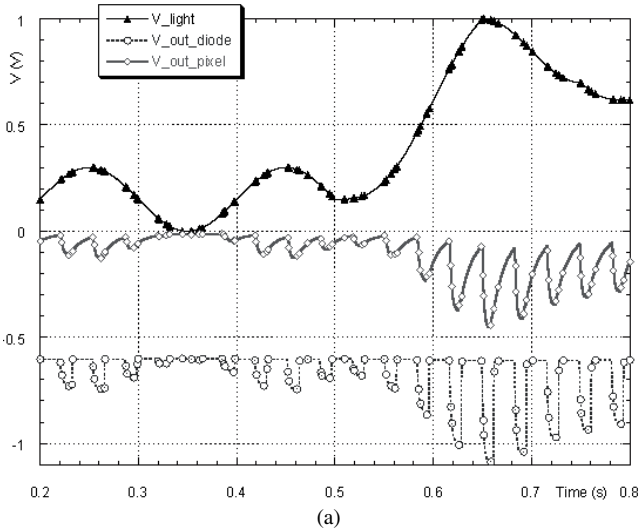

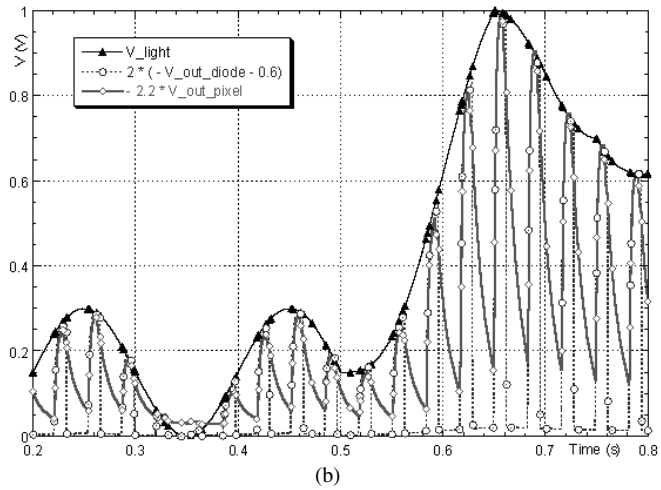

Fig. 12. (a) V_light, V_out_photodiode and V_out_pixel signals for the proposed 3 CMOS structure pixel; (b) V_out_photodiode and V_out_pixel scaled to the V_light level in order to see the correlation between light excitation and the response of the pixel.

the tunnel and the Poole-Frenkel effects, which describe the decrease of the energy barrier to emission by a voltage. The proposed SPICE model for the a-Si:H p^+-i-n^+ photodiode represents properly the dynamics of the polarization voltage. In particular, the model allows the simulation of $I(V)$ characteristics, both in dark and illumination conditions, which fit well with the corresponding experimental ones. The model also proves its validity to the study of the static behaviour.

Clear insights into the aspects that make the model correspond considerably to reality are given by precise definition of the photodiode work zone.

The successful integration of the photodiode model within a pixel structure proves the interest for further developments, such as the complete implementation of a whole sensor circuit.

Finally, we wish to express our belief that this paper provides the reader not only with a good and simple SPICE p^+-i-n^+ photodiode model, but also with a clearer understanding of the link between experiment, scientific validation and development in practical applications in the context of a laboratory study.

References

1. S. Tchakarov, P. Roca, I. Cabarrocas, U. Dutta, P. Chatterjee, B. Equer, J. Appl. Phys. **94**, 7317 (2003)
2. S. Tchakarov, U. Dutta, P. Roca i Cabarrocas, P. Chatterjee, J. Non-Cryst. Sol. **338**, 766 (2004)
3. C. Guedj, N. Moussy, W. Rabaud, P. Roca I Cabarrocas, S. Tchakarov, J.P. Kleider, J. Non-Cryst. Sol. **338**, 749 (2004)
4. J.A. Theil, R. Snyder, D. Hula, K. Lindahl, H. Haddad, J. Roland, J. Non-Cryst. Sol. **299**, 1234 (2002)
5. P.W. Tuinenga, *SPICE, guide pour l'analyse et la simulation de circuits avec PSPICE* (Masson de Paris, Prentice Hall London, 1994)
6. R. Kielkowski, *SPICE, practical device modeling* (McGraw-Hill Inc., 1995)
7. J. Frenkel, Phys. Rev. **54**, 647 (1938)
8. G. Vincent, A. Chantre, D. Bois, J. Appl. Phys **50**, 5484 (1979)
9. F. Lemmi, J. Non-Cryst. Sol. **266**, 1198 (2000)
10. B. Equer, A. Ilie, J. Non-Cryst. Sol. **190**, 67 (1995)